



1 **Measurement report: Atmospheric mercury in a coastal city of**  
2 **Southeast China: inter-annual variations and influencing factors**

3 Jiayan Shi<sup>1,2,4</sup>, Yuping Chen<sup>1,2,3</sup>, Lingling Xu<sup>1,2,\*</sup>, Youwei Hong<sup>1,2</sup>, Mengren Li<sup>1,2</sup>, Xiaolong Fan<sup>1,2</sup>, Liqian  
4 Yin<sup>1,2</sup>, Yanting Chen<sup>1,2</sup>, Chen Yang<sup>1,2,3</sup>, Gaojie Chen<sup>1,2,3</sup>, Taotao Liu<sup>1,2,3</sup>, Xiaoting Ji<sup>1,2,3</sup>, Jinsheng Chen<sup>1,2,\*</sup>

5

6 <sup>1</sup> Center for Excellence in Regional Atmospheric Environment, Institute of Urban Environment, Chinese  
7 Academy of Sciences, Xiamen 361021, China

8 <sup>2</sup> Key Lab of Urban Environment and Health, Institute of Urban Environment, Chinese Academy of  
9 Sciences, Xiamen 361021, China

10 <sup>3</sup> University of Chinese Academy Sciences, Beijing 100049, China

11 <sup>4</sup> College of Resources and Environment, Fujian Agriculture and Forestry University, Fuzhou 350002,  
12 China

13

14 **Correspondence:** Lingling Xu ([linglingxu@iue.ac.cn](mailto:linglingxu@iue.ac.cn)) and Jinsheng Chen ([jschen@iue.ac.cn](mailto:jschen@iue.ac.cn))

15

16

17

18

19

20

21

22

23

24

25

26

27



28 **Abstract.** Long-term monitoring of atmospheric mercury is an important part of the effective evaluation  
29 of the Minamata Convention on Mercury. Gaseous elemental mercury (GEM) along with conventional  
30 air pollutants and meteorological parameters were simultaneously observed in Xiamen city, Southeast  
31 China in January and July over the period 2012 – 2020. GEM concentrations in January slightly increased  
32 from 2012 ( $3.50 \text{ ng m}^{-3}$ ) to 2015 ( $4.47 \text{ ng m}^{-3}$ ) and then decreased to 2020 ( $3.93 \text{ ng m}^{-3}$ ), while GEM in  
33 July maintained stable from 2012 to 2017, and decreased significantly in 2020. The temporal variation  
34 of GEM was characterized by higher concentrations in winter than in summer and in nighttime than in  
35 daytime. Bivariate polar plots and HYSPLIT model were used to identify the source regions of GEM on  
36 a local and regional scale. The results indicate that GEM concentrations of air masses from all directions  
37 in January 2015 were higher than those of other years. Generalized Additive Models (GAMs), a  
38 regression analysis method, were established and applied to investigate the influencing factors on the  
39 inter-annual trend of GEM. The factors, anthropogenic emissions, meteorological conditions and  
40 transmission explained  $26.9 \pm 11.4\%$ ,  $45.7 \pm 7.2\%$  and  $27.4 \pm 6.8\%$  to the variation of GEM  
41 concentrations, respectively. Among them, the interpretation rate of anthropogenic emissions has  
42 generally decreased since 2012, whereas meteorology explained the largest proportion of GEM  
43 concentrations in almost all study periods. Our results suggest that meteorology was the more important  
44 factor, which driven the inter-annual trend of GEM in the study region.

45 **Keywords:** Inter-annual trend; Gaseous elemental mercury; GAMs; HYSPLIT model; Meteorology  
46 factors.



## 47 **1 Introduction**

48 Atmospheric mercury, because of its neurotoxicity, long persistence and high bioaccumulation, is  
49 defined as a global pollutant that poses a threat to the health of the global population. Especially the  
50 organic form of mercury, like methylmercury (MeHg), is associated with neurocognitive deficits in  
51 human fetuses and cardiovascular effects in adults (Axelrad et al., 2007; Roman et al., 2011). In order to  
52 protect human health and the environment from adverse effects of mercury, a legally-binding  
53 international treaty Minamata Convention on Mercury was adopted in October 2013 and entered into  
54 force in August 2017 (UN Environment, 2017). The Minamata Convention requires parties to reduce  
55 mercury emissions and to assess the effectiveness of mitigation measures. China is one of the world's  
56 largest mercury emitters as well as the signatory to the Minamata Convention. The annual atmospheric  
57 mercury emissions in China were about 565 tons in 2015, accounting for about a quarter of global  
58 anthropogenic mercury emissions (AMAP/UNEP, 2018). The predominant anthropogenic Hg emission  
59 sources in China were industrial coal combustion, coal-fired power plants, nonferrous metal smelting,  
60 and cement production (Zhang et al., 2015). The characteristics of Hg emissions such as large emission  
61 amount and industrial production-dominated emissions made that China has great potential to reduce  
62 mercury emissions through the implementation of the Minamata Convention on Mercury. A mercury  
63 emissions inventory of China for 1978 – 2014 has reported that anthropogenic mercury emissions peaked  
64 in 2011 and then showed a downward trend (Wu et al., 2016). In addition, China had reduced  
65 anthropogenic mercury emissions by 127 tons from 2013 to 2017 (Liu et al., 2019b). Among them,  
66 mercury emissions from the coal-fired power plants fell from 105 tons in 2007 to 73 tons in 2015 (Zhang  
67 et al., 2015; Liu et al., 2018). The main reason for this downward trend was that China has introduced a  
68 series of air cleaning measures including upgrading precipitator devices, newly built desulfurization and  
69 denitrification devices and ultra-low emission renovations since 2013, which led to synergistic removal  
70 of mercury (Liu et al., 2019b). Strict restrictions of mercury on the mining, production, utilization, import  
71 and export have also been imposed in China since 2017 (<https://www.mee.gov.cn/>, last access: 17 May  
72 2022).



73 Atmospheric mercury is usually classified into three categories according to the determination  
74 technique: gaseous elemental mercury (GEM), gaseous oxidized mercury (GOM) and particulate bound  
75 mercury (PBM). Because of its stability and volatility, GEM is the dominant form of atmospheric  
76 mercury, accounting for up to 95%. GEM has an atmospheric residence time of 0.5 – 2 years and can  
77 spread globally before being deposited to earth's surfaces (Schroeder and Munthe, 1998; Zhang et al.,  
78 2013; Yuan et al., 2021). On the other hand, GOM and PBM have relatively high reactivity and dry/wet  
79 deposition rates and are therefore easier to be removed from the atmosphere. The sum of GEM and GOM  
80 is referred as total gaseous mercury (TGM), but GOM contributed generally less than 5% of TGM  
81 (Schroeder and Munthe, 1998; Xu et al., 2020). Thus, the GEM concentrations were usually  
82 approximated to TGM concentrations. Field observations are vital to understand the long-term variation  
83 of Hg levels in the atmosphere. There are some global and regional mercury monitoring networks around  
84 the world which provided a long-term monitoring result. For example, a steep decline trend of GEM  
85 concentrations ( $0.05 \text{ ng m}^{-3} \text{ yr}^{-1}$ ) was observed at Mace Head, Ireland, from 2013 to 2018 (Custodio et  
86 al., 2020), while GEM data from Cape Point, South Africa, showed a slight increase from 2007 to 2017  
87 (Slemr et al., 2020). China has also carried out a series of observational studies in the past two decades.  
88 These observation studies on GEM concentrations mostly focused on 1 – 2 years, while few continuous  
89 GEM observation records over multiple years in China were published (Fu et al., 2015). A three-year  
90 measurement at Chongming Island, East China, showed that the annual GEM concentrations  
91 significantly decreased from  $2.68 \text{ ng m}^{-3}$  in 2014 to  $1.60 \text{ ng m}^{-3}$  in 2016, at a rate of  $-0.60 \pm 0.08 \text{ ng m}^{-3}$   
92  $\text{yr}^{-1}$  (Tang et al., 2018). Whereas, a multi-year observation of GEM in Guiyang, Southwest China,  
93 showed an increasing trend from  $8.40 \text{ ng m}^{-3}$  in 2002 to  $10.2 \text{ ng m}^{-3}$  in 2010, and the increase mainly  
94 occurred during the cold season (Fu et al., 2015).

95 The variation of GEM concentrations is influenced by a variety of factors such as anthropogenic  
96 emissions, meteorological conditions, as well as intra- and inter-regional transport (Tang et al., 2018; Liu  
97 et al., 2019a; Zhang et al., 2021). In previous studies, the impact of anthropogenic emissions changes  
98 was often quantified by compiling emission inventories (Zhang et al., 2015; Wu et al., 2016; Liu et al.,  
99 2019b; Cai et al., 2020). The trajectory-based analysis method was frequently applied to analyze the  
100 impact of regional transport (Tang et al., 2018; Wang et al., 2021). However, the results like the impacts



101 of anthropogenic emissions and regional transport derived from above different method systems could  
102 not be comparable. Generalized additive models (GAMs) have been introduced into influencing factor  
103 identification in recent years, which are data-driven and able to incorporate non-linear relationships of  
104 air pollution with numerical and categorical variables (Wood and Augustin, 2002). The impact of local  
105 anthropogenic emissions, regional transport, and meteorological factors on GEM concentrations in  
106 Nanjing, East China was quantified by using the GAMs (Zhang et al., 2021). GAMs were also used to  
107 explain the decline of GEM concentrations in Beijing and the result showed that reduction of  
108 anthropogenic mercury emissions, variation in meteorological conditions, and change in globe  
109 background level explained 51.5%, 47.1% and 1.4% of the decrease of GEM concentrations, respectively  
110 (Wu et al., 2020). It can be seen that GAMs are a promising tool to explore the effect of factors like  
111 anthropogenic emissions and natural perturbations on GEM concentrations.

112 China has adopted aggressive atmospheric control measures in the last decade. Long-term GEM  
113 observation was very necessary to investigate the variation of GEM levels and its influencing factors. In  
114 this study, GEM, conventional pollutants and meteorological parameters were simultaneously observed  
115 in Xiamen, a coastal city in Southeast China, in January (represents winter) and July (represents summer)  
116 over the period 2012 – 2020. The main objectives of this study are: (1) to characterize the inter-annual,  
117 seasonal and diurnal variations of GEM in a coastal city of Southeast China, (2) to identify the source  
118 regions of GEM on a local and regional scale and their influence on annual concentrations of GEM, (3)  
119 to investigate the influencing factors including anthropogenic emissions, regional transport and  
120 meteorology on the inter-annual variation of GEM concentrations.

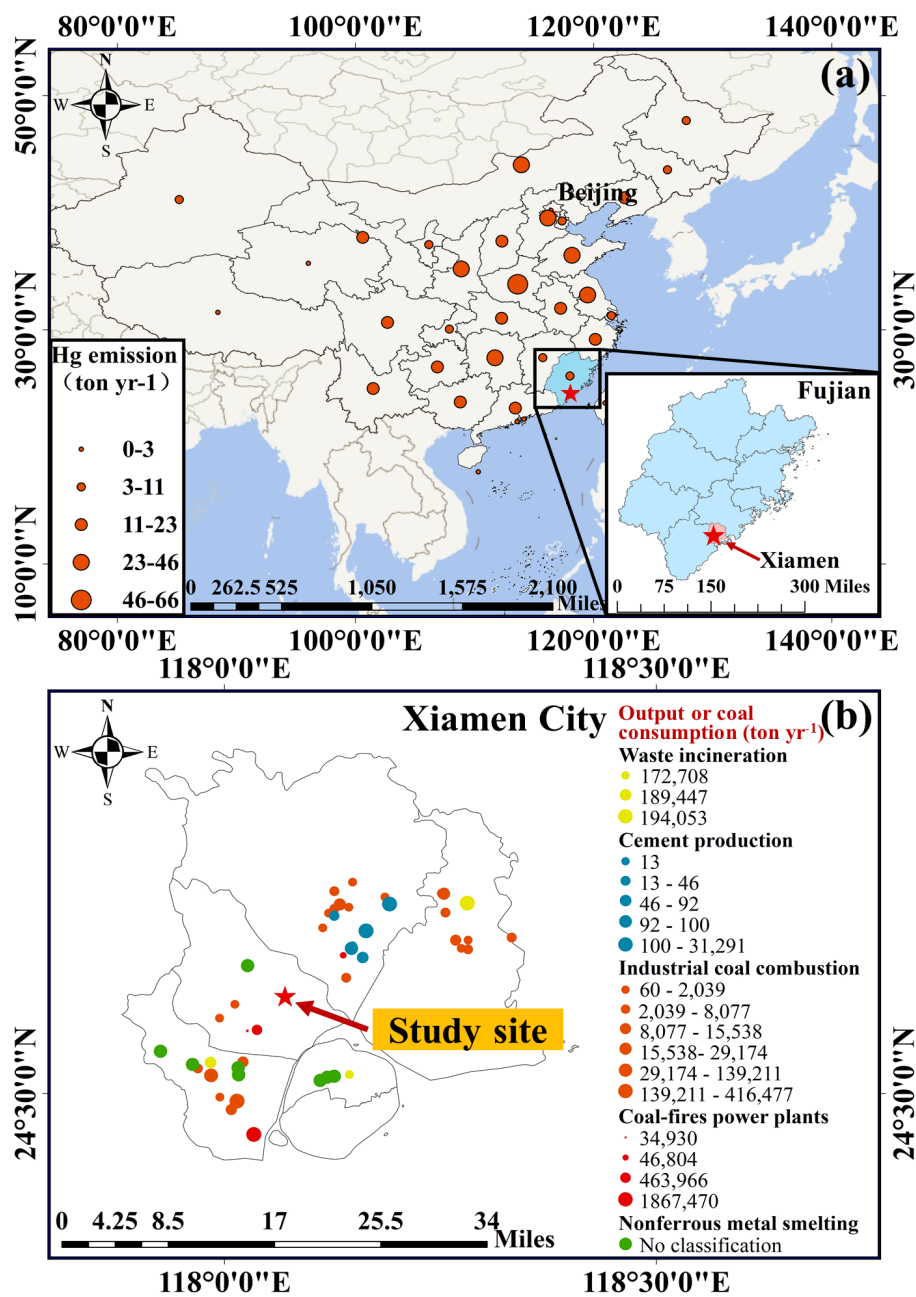
## 121 **2 Method**

### 122 **2.1 Site description**

123 The study site (Xiamen, 118°04'13''E, 24°36'52''N) is located in the Institute of Urban Environment,  
124 Chinese Academy of Sciences in Jimei District of Xiamen City, Fujian Province, China (Fig. 1a). The  
125 site was characterized by a typical subtropical monsoon climate, with the prevailing ocean monsoon in  
126 summer and northerly or northeasterly winds from the inland of China in winter. Industrial point sources  
127 were mainly distributed to the northeast and the southwest of the study site (Fig. 1b). The instruments



128 were placed on the roof of a building (~80 m above the ground). The outdoor air inlet of the sampling  
129 unit was located at 2 m above the rooftop of the building.



130  
131 **Figure 1.** (a) The location of study site in Xiamen City, Fujian Province, China and the regional distribution  
132 map of anthropogenic Hg emissions in China in 2014 (Wu et al., 2016). Note that the red dots represent the



133 amount of mercury emitted by each province. (b) The distribution of local industrial point sources in Xiamen.  
134 Note that the colors of the dots represent different industrial categories, and the size represents a company's  
135 output or coal consumption (ton yr<sup>-1</sup>).

## 136 2.2 Atmospheric mercury measurements

137 Atmospheric mercury was measured by the Tekran 2537B/1130/1135 system (Tekran Inc., Toronto,  
138 Canada). Continuous 5 min of GEM concentrations were measured by a Tekran 2537B Hg vapor analyzer,  
139 with a detection limit of 0.06 ng m<sup>-3</sup> at a sampling flow rate of 1 L min<sup>-1</sup> (Tekran, 2001; Xu et al., 2015).  
140 The principle and the routine maintenance of the equipment in detail have been described in the previous  
141 study (Xu et al., 2015). The Tekran 2537B analyzer was calibrated automatically every 25h using the  
142 internal Hg permeation source inside the instrument, and the accuracy of this permeation source was  
143 calibrated every 12 months with manual injection of Hg by a syringe from an external Hg source (Module  
144 2505). This study was based on the GEM observation data of January and July (representative of winter  
145 and summer, respectively) in 2012, 2013, 2015, 2017 and 2020. Gap years in GEM data were generally  
146 due to abnormal operation of the instrument or mismatch observation periods. In order to match other  
147 parameters, the time resolution of GEM concentrations was converted from the original 5 min to 2 h. The  
148 proportion of GOM in Xiamen was less than 5% of the TGM during the study period. Thus, GEM  
149 concentrations in this study were directly compared to TGM in the below analysis.

## 150 2.3 Meteorological parameters and criteria air pollutants

151 In this study, the conventional pollutants (including SO<sub>2</sub>, NO<sub>2</sub>, O<sub>3</sub>, CO, PM<sub>10</sub>, PM<sub>2.5</sub>) and  
152 meteorological parameters (including wind speed (WS), wind direction (WD), relative humidity (RH),  
153 air temperature (*T*) and surface air pressure (SP)) were obtained from Xiamen air quality monitoring  
154 station. Note that above pollutants concentrations and meteorological data were averaged into 2 h time  
155 intervals. Other meteorological parameters: boundary layer height (BLH), downward UV radiation at the  
156 surface (UVB) and low cloud cover (LCC) were obtained from the European Centre for Medium-Range  
157 Weather Forecasts (ECMWF) reanalysis (<https://www.ecmwf.int>, last access: last access: 23 March  
158 2022).



## 159 2.4 Potential source regions identification

160 Hybrid Single-Particle Lagrangian Integrated Trajectory (HYSPPLIT) model and Global Data  
161 Assimilation System data (<https://www.arl.noaa.gov/>, last access:5 May 2022) were applied to calculate  
162 the 72h backward air mass trajectories. The interval of backward trajectories was 2 h and the arrival  
163 height was set as 500 m above the ground level. Total spatial variance (TSV) method was chosen to  
164 calculate clusters in the HYSPPLIT calculation (Draxler, 1999). The clusters of air mass trajectories were  
165 further categorized into five potential source regions in January and four source regions in July according  
166 to their travel paths. For example, air parcels which originated from Fujian province over the last 3 d  
167 were considered to be local air masses named Local (the details of the source region definition are  
168 presented in Support Information). The observed GEM concentrations were assigned to the trajectories.  
169 The mean GEM concentration related to each potential source region ( $C_i$ ) was calculated by Equation  
170 (1). The weighted GEM concentration contribution ( $W_{Regions}$ ) of each source region to the observed  
171 average GEM was calculated by Equation (2):

$$C_i = \frac{\sum_{l=1}^{M_i} C_l}{M_i}, \quad (1)$$

$$W_{Regions} = \frac{\sum_{l=1}^{M_i} C_l}{\sum_{i=1}^n C_i \times M_i}, \quad (2)$$

172 Where  $i$  is the index of the source regions,  $l$  is the index of the trajectory,  $M_i$  is the total number of  
173 trajectories originated from the  $i$  source regions,  $C_l$  is GEM concentration observed upon arrival of  
174 trajectory  $l$ ,  $n$  is the number of all source regions over each time period.

## 175 2.5 Model development

176 Generalized Additive Models, a regression analysis method, have been used to establish the  
177 relationship between GEM and various variables, and to investigate the influencing factors on the inter-  
178 annual trend of GEM concentrations (Gong et al., 2017). The models were run by the following steps:  
179 model establishment, parameter selection and model quality control.

180 **Model Establishment:** GAMs were performed using R version 4.1.2 with the “mgcv” package. The  
181 equation can be described as follows:



$$g(\mu) = f_1(x_1) + f_2(x_2) + \dots + f_k(x_k) + \varepsilon, \quad (3)$$

182 Where  $x_j$  ( $j = 1, 2, 3, \dots, k$ ) are different meteorological predictors and  $f_j$  is a smooth function of the  
183 predictors;  $\varepsilon$  is the residual;  $\mu$  is the expected value of the response variable; and  $g$  is the link function  
184 specifies the relationship between the non-linear formulation and the expected value. We used the  
185 "identity link" function with a Gaussian distribution because the relationship between GEM and the  
186 variables conformed to a Gaussian distribution and the estimation of GAMs was considered unbiased. In  
187 order to ensure the balance between under-fitting and overfitting of observation data, we used a penalized  
188 cubic regression as a smooth function. In the running process of the model, the concentration contribution  
189 of the smoothed independent variable to the dependent variable was output and converted into  
190 contribution ratio, which is helpful to determine the degree of each variable driving the prediction.

191 **Parameter Selection:** In this study, 16 variables accompanied with GEM concentrations were used  
192 for GAMs establishment. These variables were divided into four categories: anthropogenic emissions  
193 ( $\text{SO}_2$ ,  $\text{NO}_2$ ,  $\text{O}_3$ ,  $\text{CO}$ ,  $\text{PM}_{2.5}$ ,  $\text{PM}_{10}$ ), surface meteorology ( $T$ ,  $\text{RH}$ ,  $\text{WS}$ ,  $\text{WD}$ ,  $\text{SP}$ ), high-altitude  
194 meteorology ( $\text{BLH}$ ,  $\text{UVB}$  and  $\text{LCC}$ ) and air transmission (24h-Latitude and 24h-Longitude) (Table S1).  
195 In order to eliminate the significant colinearity variables, the colinearity diagnosis method was adopted  
196 to make judgment according to the variance inflation factor (VIF). The performance of GAMs was judged  
197 according to Akaike Information Criterion (AIC) and  $R^2$  values. Specifically, as the parameters were  
198 successively added into the model, the AIC decreased and  $R^2$  increased. Based on this method, 5 variables  
199 including  $\text{CO}$ ,  $\text{RH}$ ,  $\text{SP}$ , 24h-Latitude and 24h-Longitude were eventually selected into the model (Table  
200 S2). Given that the main anthropogenic sources of GEM in China are combustion (Liu et al., 2019b; Wu  
201 et al., 2020),  $\text{CO}$  was used to represent the anthropogenic Hg emissions factor.  $\text{RH}$  and  $\text{SP}$  were classified  
202 as the meteorological factor, and 24h-Latitude and 24h-Longitude represented the transmission factor  
203 (Wu et al., 2020). Given that five selected variables passed the colinearity test, the three factors in the  
204 model were considered to be independent of each other.

205 **Model Quality Control:** The accuracy of GAMs simulation was assessed using a 10-fold cross-  
206 validation test. The principle of the test is dividing the whole dataset into ten subsets randomly, and in  
207 each round of cross-validation, nine subsets are used to fit the model and the remaining one is predicted.  
208 This process is repeated 10 times to ensure that every subset is tested. The 10-fold cross-validation results



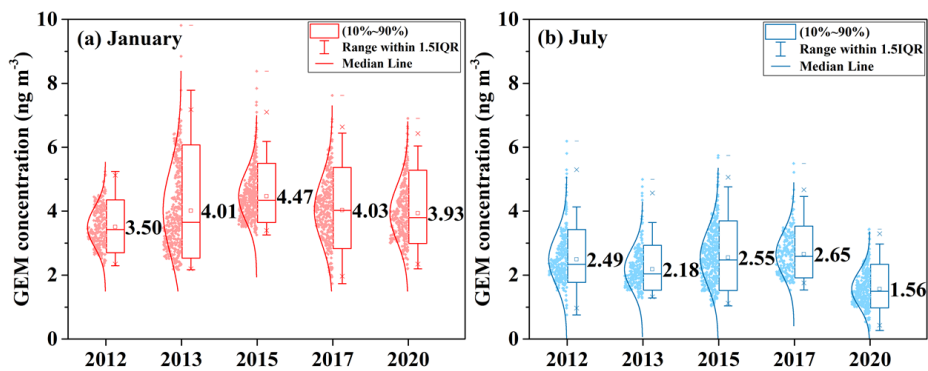
209 showed a good coincidence between the GAMs and cross-validated results ( $R^2 = 0.97$ , Fig. S1),  
210 demonstrating the reliability of the established model. In order to test the underlying assumptions of  
211 homogeneity, normality and independence of GAMs to ensure the validity and accuracy of the model,  
212 we used the following methods (Fig. S2): (1) Quantile-quantile (QQ) plots (Sample quantiles against  
213 theoretical quantiles), (2) scatterplots (residuals against linear predictor), (3) histograms of the residuals  
214 and (4) scatter plots (response against fitted value). The QQ-plot showed that the GAMs produced good  
215 results around the average concentrations and the residuals showed a normal distribution. The fitted GEM  
216 and observed GEM were also compared to further valid the accuracy of the established model.

## 217 **3 Results and discussion**

### 218 **3.1 Temporal variations of GEM concentrations**

#### 219 **3.1.1 Inter-annual variation**

220 Monthly concentrations of GEM ranged from 3.50 to 4.47  $\text{ng m}^{-3}$  in January and 1.56 to 2.65  $\text{ng m}^{-3}$   
221 in July during the whole study period, with mean values of  $4.04 \pm 1.01 \text{ ng m}^{-3}$  and  $2.29 \pm 0.83 \text{ ng m}^{-3}$ ,  
222 respectively. The GEM concentrations in Xiamen were several times higher than the Hemisphere  
223 background concentrations (about 1.5 – 1.7  $\text{ng m}^{-3}$ ) (Lindberg et al., 2007; Sprovieri et al., 2010).  
224 Comparisons of TGM/GEM concentrations in Xiamen with other urban and rural areas in East Asia over  
225 the last decade are shown in Table 1. The mean concentrations of GEM mostly fell in a range of 2 – 5  $\text{ng}$   
226  $\text{m}^{-3}$  in East Asia (except for some background sites). The GEM in Xiamen was slightly higher than those  
227 measured at rural and background monitoring sites such as Tibetan Plateau region, Mt. Changbai, and  
228 Mt. Ailaoshan (Zhang et al., 2016a; Yin et al., 2018; Liu et al., 2019a), while lower than those reported  
229 from inland urban sites like Lanzhou, Nanjing, and Shanghai (Zhu et al., 2012; Duan et al., 2017; Yin et  
230 al., 2020).



231

232 **Figure 2. Statistical summaries of gaseous elemental mercury (GEM) concentrations in Xiamen in (a) January**  
233 **and (b) July of the study years.**



234

**Table 1. Comparisons of TGM/GEM concentrations in Xiamen with other urban and rural areas in East Asia over the period 2010 – 2020.**

Locations	Classification	Time	TGM/GEM (ng m <sup>-3</sup> )	Winter	Summer	References
Xiamen, CN	Suburban (Coast)	03/2012–02/2013	3.50±1.21	/	/	(Xu et al., 2015)
Mt. Changbai, CN	Rural	07/2013–07/2014	1.68±0.47	/	/	(Liu et al., 2019a)
Haidian, CN	Urban	02/2018–03/2018	2.77±0.91	/	/	(Wang et al., 2021)
Shanghai, CN	Suburban	06/2014–12/2014	4.19±9.13	5.5±6.6	3.8–5.3	(Duan et al., 2017)
Shanghai, CN	Suburban	12/2015–02/2016	2.77±1.36	2.88	2.87	(Qin et al., 2019)
Hefei, CN	Suburban	07/2013–06/2014	4.07±1.91	4.05 ± 1.81	4.08±1.99	(Hong et al., 2016a)
Ningbo, CN	Coastal	04/2011–04/2013	3.30±1.40	3.70	2.60	(Yu et al., 2015)
Ningbo, CN	Urban (Coastal)	07/2013–01/2014	3.26±1.63	/	/	(Hong et al., 2016b)
Ningbo, CN	Urban (Coastal)	12/2016–11/2017	2.44±0.95	2.62±1.05	2.26±0.78	(Yi et al., 2020)
Nanjing, CN	Urban	01/2011–12/2011	7.94±6.99	5.5±2.5	9.9±8.2	(Zhu et al., 2012)
Mt. Ailaoshan, CN	Rural	05/2011–05/2012	2.09±0.63	2.04±0.58	2.20±0.60	(Zhang et al., 2016a)
Taoyuan city, Taiwan, CN	Suburban	10/2017–09/2018	2.61±6.47	2.19±0.75	2.27±1.67	(Sheu et al., 2019)
Taichung city, Taiwan, CN	Rural	10/2014–09/2015	1.19	/	/	(Fang et al., 2017)
Yongheung, Korea	Island	01/2013–08/2014	2.80±1.10	3.50–3.70	2.30±0.90	(Lee et al., 2016)
Gyodong Island, Korea	Rural	08/2015–09/2017	2.70±2.60	2.8±2.9	1.70±1.0	(Lee et al., 2019)
Fukuoka, Japan	Urban	06/2012–05/2013	2.33±0.49	2.31±0.44	2.37±0.58	(Marumoto et al., 2015)
Nam Co, Tibetan Plateau, CN	Plateau	01/2012–10/2014	1.33±0.24	1.14±0.18	1.50±0.20	(Yin et al., 2018)
Changdao Island, CN	Rural (Coastal)	10/2013–07/2015	2.52±0.82	2.87±1.16	2.25±0.51	(Wang et al., 2020)
Lanzhou, CN	Urban	10/2016–10/2017	4.48±2.32	5.06±2.45	4.45±2.10	(Yin et al., 2020)



235 The inter-annual variability of GEM concentrations in January and July are shown in Fig. 2. The GEM  
236 concentrations in Xiamen showed no distinct trends over the period 2012 – 2020. Specifically, GEM  
237 concentrations in January displayed a slight upward trend from 2012 ( $3.50 \text{ ng m}^{-3}$ ) to 2015 ( $4.47 \text{ ng m}^{-3}$ )  
238 and a decreasing trend from 2015 to 2020 ( $3.93 \text{ ng m}^{-3}$ ). Whereas GEM concentrations in July were stable  
239 from 2012 to 2017, and decreased significantly in 2020. Hg emission inventories showed that the total  
240 anthropogenic Hg emissions in China were mitigated during the last decade and the inflection point was  
241 most likely to occur between 2010 and 2015 (Zhang et al., 2015; Wu et al., 2016; Liu et al., 2018; Liu et  
242 al., 2019b). Recent studies have indicated either a stable or a slight decreasing trend for GEM or TGM  
243 concentrations in Chinese cities after 2013 when China has applied the aggressive measures to control  
244 air pollution (Qin et al., 2020; Wu et al., 2020; Yin et al., 2020). For instance, it was reported that GEM  
245 concentrations at Chongming Island in East China significantly decreased from 2014 to 2016, and the  
246 inflection point occurred before 2014 (Tang et al., 2018). Note, those measurements mostly lasted for 2  
247 – 4 years. So far, the observations of GEM concentrations over a long time period were scarce. Our result  
248 suggests the influencing factors on the variation trend of GEM in East China would be complex over the  
249 last decade.

250 Coal combustion is one of the leading mercury sources in China (Wu et al., 2006). Table S3 summaries  
251 the consumption of coal and the statistics of annual  $\text{SO}_2$  and  $\text{NO}_x$  emissions in Fujian Province over the  
252 period 2012 – 2020. The coal consumption in Fujian Province showed a small fluctuation among years.  
253 Whereas, there was a decreasing trend for  $\text{SO}_2$  and  $\text{NO}_x$  emissions from 2013 to 2017 with the air  
254 pollution control measures implemented in China. Previous studies have found that mercury can be  
255 synergistically removed in the process of desulfurization and de-nitration (Zhang et al., 2016b; Liu et al.,  
256 2019b). The installation of selective catalytic reduction to control nitrogen oxide emissions is often  
257 accompanied by the oxidation of GEM to GOM, and the combined application of selective catalytic  
258 reduction and flue gas desulfurization could further reduce TGM emissions to the atmosphere (Rallo et  
259 al., 2012). Nonetheless, the inconsistent inter-annual trend in GEM concentrations and  $\text{SO}_2/\text{NO}_x$   
260 emissions indicates that additional factors, like GEM emission sources other than coal combustion and/or  
261 meteorological changes drove the inter-annual variation trend of GEM in the study region.



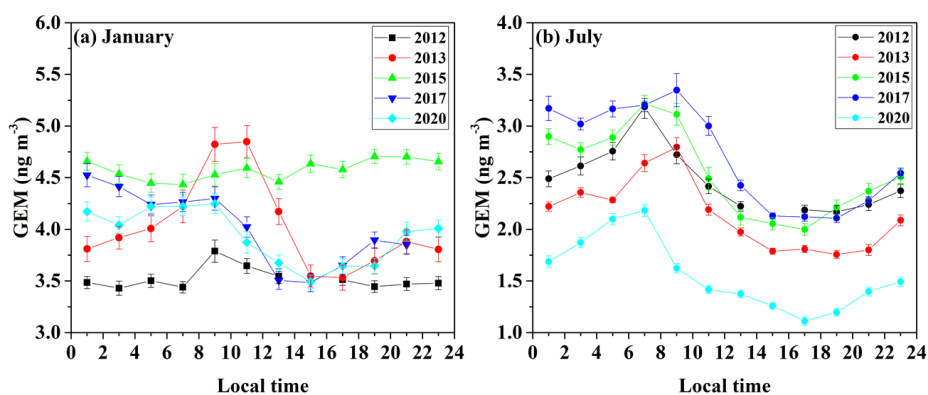
### 262 3.1.2 Seasonal and diurnal patterns

263 The GEM concentrations in Xiamen were approximately 1.41 – 2.52 times higher in winter than in  
264 summer ( $P < 0.001$ , one-way ANOVA) over the study years. The similar seasonal variation was widely  
265 observed in cities including Shanghai, Ningbo, Lanzhou, and Yongheung, as well as Gyodong Island,  
266 and Changdao Island (Yu et al., 2015; Hong et al., 2016b; Lee et al., 2016; Duan et al., 2017; Lee et al.,  
267 2019; Wang et al., 2020; Yi et al., 2020; Yin et al., 2020). However, a reverse seasonal variation with  
268 higher GEM in summer than in winter was observed in Nanjing, Chongming Island, Mt. Ailaoshan and  
269 Tibetan Plateau region (Zhu et al., 2012; Zhang et al., 2016a; Tang et al., 2018; Yin et al., 2018). There  
270 were many factors responsible for the seasonal variation of GEM in Xiamen. In terms of Hg emission  
271 sources, local industrial emissions were relatively stable over the course of a year. The key factor with  
272 seasonal changes is the increased usage of coal for heating which mainly occurred in northern China in  
273 cold seasons. Although there was no coal consumption for heating in southern China, GEM is well mixed  
274 due to its prolonged lifetime (0.5 – 1 year) (Qiu et al., 2021). Monsoonal winds can change the source–  
275 receptor relationships at observation sites, and thus affect the seasonal variation of GEM concentrations  
276 (Fu et al., 2015; Liu et al., 2019a). Winter winds in Xiamen mainly originated from north directions  
277 which passed through numerous intensive anthropogenic GEM emissions areas (Fig. 1a), while summer  
278 winds mainly originated from ocean with less GEM point sources. Another important factor is that the  
279 mixing heights were reduced due to stable inversion layer in winter. As a result, GEM diffused slowly  
280 and accumulated easily in the surface layer. In addition, for the sites in the Northern Hemisphere, the  
281 greater removal of GEM by wet and dry deposition could also lead to lower GEM concentrations in  
282 warmer seasons (Fu et al., 2008; Tang et al., 2018).

283 The diurnal variations of bihourly GEM concentrations were consistent among years (Fig. 3). The  
284 GEM concentrations generally displayed a downward trend during the day and an accumulation trend  
285 over time at night, with a peak at 8:00 – 10:00 am and a valley at 14:00 – 16:00 pm. Among them, GEM  
286 concentrations in January 2015 were relatively high on the whole, and the diurnal change of GEM  
287 concentrations was gentle, which might be related to the enhanced transport of continental pollution from  
288 northeast Asia due to the extreme 2015 – 2016 El Niño event (Fu et al., 2012; Nguyen et al., 2022). The  
289 diurnal pattern of GEM concentrations in Xiamen is consistent with other urban sites like Guiyang, Hefei



290 and Guangzhou (Feng et al., 2004; Chen et al., 2013; Fu et al., 2015). Previous studies often attributed  
291 diurnal variations of GEM to the effect of various anthropogenic emissions, photochemical oxidation  
292 and the diurnal variation of BLH (Hong et al., 2016b; Duan et al., 2017). The diurnal pattern of GEM in  
293 Xiamen was similar to those of SO<sub>2</sub>, NO<sub>2</sub> and CO (Fig. S3a – c), reflecting the combined effects of  
294 common anthropogenic emissions and the diel fluctuation in meteorology such as the BLH. The  
295 decreasing trend of GEM from early morning to afternoon was due to the intensified turbulent mixing in  
296 the boundary after sunrise while the nighttime had the opposite condition (Fig. S3e). In addition, the  
297 GEM concentrations decreased during the daytime with the increase of O<sub>3</sub> (Fig. S3d). Thus, we could  
298 expect that the photo-oxidation of GEM to GOM partly reduced the GEM concentrations after morning.



299  
300 **Figure 3. The diurnal trend of GEM concentrations in (a) January and (b) July over the study years. Note**  
301 **that the value of error bars has been reduced tenfold.**

### 302 3.2 Potential source regions of GEM

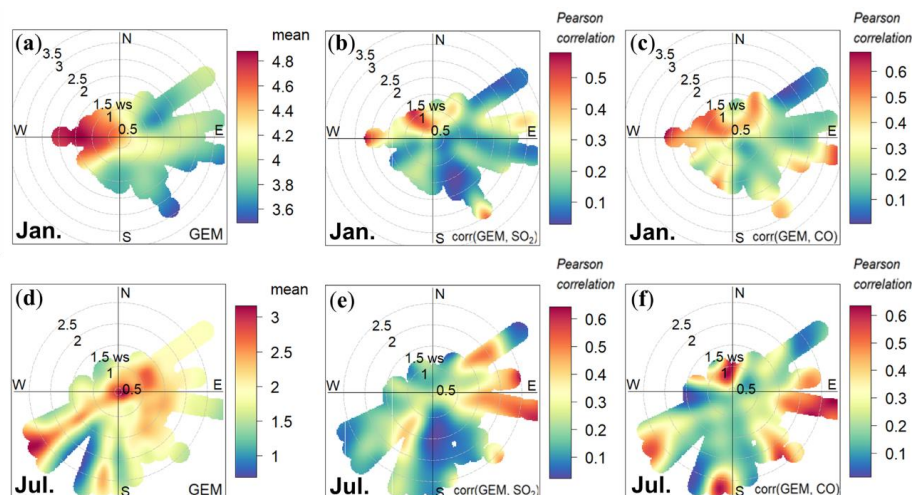
#### 303 3.2.1 Local emissions

304 According to the industrial Hg emissions inventory in China, the main Hg emissions industries  
305 included industrial coal combustion, coal-fired power plants, non-ferrous metal smelting, cement  
306 production, and waste incineration (Zhang et al., 2015; Wu et al., 2016). The relationships between the  
307 spatial distribution of industrial sources and bivariate polar plots of GEM concentrations would shed  
308 light on the influence of local anthropogenic point sources on GEM concentrations. As shown in Fig.4a,  
309 4d, the elevated GEM concentrations in the bivariate polar plots of individual seasons were highly  
310 concentrated, suggesting that the spatial distribution of main Hg point sources was similar among years.



311 However, the polar plot results of GEM concentrations were distinctly different between seasons likely  
312 due to the shift in the wind. In January, the elevated GEM concentrations were associated with west wind  
313 with a low WS of  $0.5 - 2.0 \text{ m s}^{-1}$  (Fig. 4a), which indicates nearby emission sources. They were likely  
314 the industrial coal combustion, and non-ferrous metal smelting upwind from the west of the monitoring  
315 site (Fig. 1b). The conventional pollutants are the good indicators of primarily anthropogenic sources. In  
316 Xiamen city, the coal-fired power plants contributed 62% of local  $\text{SO}_2$  emissions and 57% of CO  
317 emissions. A close correlation of GEM with  $\text{SO}_2$  and CO in westerly WD with low speeds (Fig. 4b, 4c)  
318 further supported above conclusion that the contributions of local industrial sources to GEM.

319 In July, the elevated GEM concentrations occurred when winds came from the southwest with the WS  
320 about  $2.5 - 3 \text{ m s}^{-1}$  (Fig. 4d). As shown in Fig. 1b, there are many industrial clusters in the southwest  
321 direction of the observation site including coal-fired power plants, industrial coal combustion and  
322 nonferrous metal smelting. Accordingly, we suspected that the local industrial clusters upwind of the  
323 southwest to the study site caused an evident increase in GEM concentrations. High WS of the southwest  
324 wind likely weakened the correlation between GEM and  $\text{SO}_2$  (Fig. 4e) while GEM and CO remained a  
325 good correlation in the southwest wind due to their stable chemical properties (Fig. 4f). Another elevated  
326 GEM concentration condition occurred when wind came from the east with a lower WS of  $0 - 2 \text{ m s}^{-1}$   
327 (Fig. 4d). Such low WS suggests a stagnant meteorological condition which was unfavorable for GEM  
328 dispersion. In addition, GEM and  $\text{SO}_2$  showed a good correlation in the case of the east wind with WS  
329 of  $1 - 2 \text{ m s}^{-1}$ . Hence, we could speculate that the upwind point sources, like industrial coal combustion  
330 and nonferrous metal smelting, as well as the adverse atmospheric diffusion conditions contributed to the  
331 increasing GEM concentrations. As shown in Table S4, GEM in Xiamen was overall positively correlated  
332 with  $\text{SO}_2$ ,  $\text{NO}_2$ , CO and  $\text{PM}_{2.5}$ , but the correlation coefficient fluctuated remarkably among years. In  
333 addition, the inter-annual trend of GEM concentrations was not coincided with those of  $\text{SO}_2$  or  $\text{NO}_x$   
334 emissions as mentioned above. Thus, although local Hg point sources contributed to the elevated GEM  
335 concentrations in individual seasons, they might be not the dominant factor on the inter-annual trend of  
336 GEM concentrations in the study region.



337

338 **Figure 4.** Bivariate polar plots of GEM concentrations (a, d), the correlation coefficients of GEM with SO<sub>2</sub> (b,  
339 e) and CO (c, f) as a function of WS and WD in January and July during the whole study period. Note that  
340 GEM in ng m<sup>-3</sup>, wind speed in m s<sup>-1</sup>, wind direction in °.

### 341 3.2.2 Long distance migration

342 The clusters of 72 h air mass backward trajectories and the potential source regions of GEM in January  
343 and July during the study years are shown in Fig. 5. On the whole, the GEM concentrations in Xiamen  
344 were under an influence of continental air masses in January and a mixing influence of continental and  
345 marine air masses in July. According to the direction of air mass trajectory clusters, the source regions  
346 of GEM in January were classified to the local region (Local), East China (EC), Southwest China (SWC),  
347 North China (NC) and Central China (CC). It can be seen that air masses from the Local and EC  
348 dominated in January, which accounted for 60.6% – 100% of the total trajectories over the study years.  
349 The GEM concentrations in Xiamen were also affected by the long-distance transport of air masses from  
350 Mongolia through the NC in January of 2013, 2015 and 2020 and from the SWC in January of 2015,  
351 2017 and 2020. Table 2 summarizes the mean concentrations and weighted average contributions of  
352 GEM associating with different backward trajectory clusters in January and July. The GEM in January  
353 were mainly contributed by the Local and EC with the weighted average contributions more than 75%  
354 (except 2017 that was influenced by the CC). The results could reasonably be expected because  
355 anthropogenic Hg emissions in East China was extremely large due to the dense industries (Zhang et al.,  
356 2015). The North China Plain region was one of the heaviest mercury polluted area in China (Zhang et



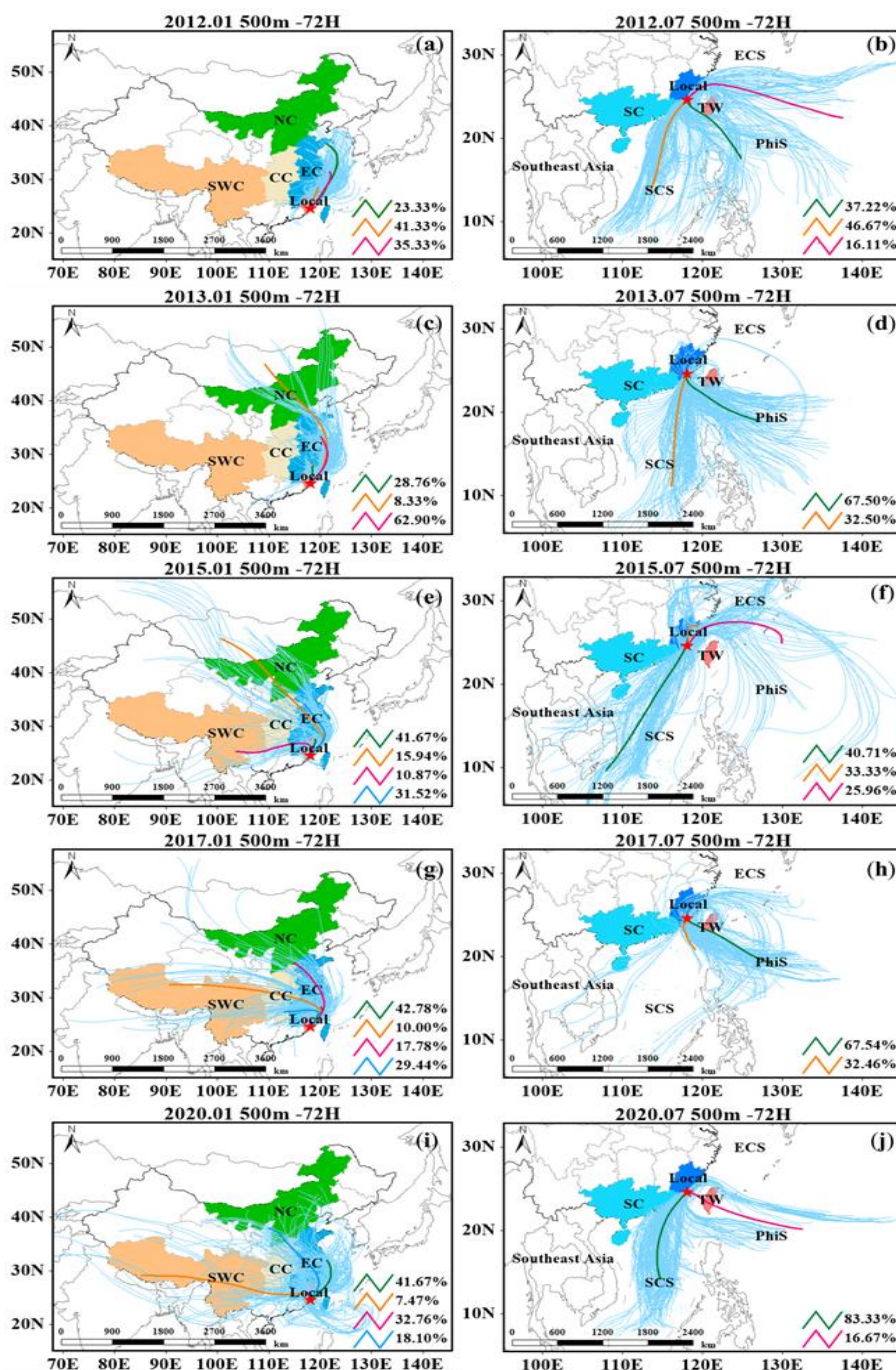
357 al., 2015). But to our surprise, the GEM concentrations associated with air masses from the NC were  
358 relatively low compared to air masses from other directions. This is most likely due to the effect of  
359 transmission distances, while GEM concentrations decreased with long transport distances. In contrast,  
360 short air mass trajectories, like from the Local, indicated a relatively stagnant air condition which is not  
361 conducive to the diffusion of GEM (Zhang et al., 2021). The GEM concentrations of air masses from all  
362 directions in 2015 were higher than those of other study years (Table 2). Previous studies have also  
363 reported the high levels of GEM in 2015 among urban Beijing, Changdao Island, rural Shanghai and  
364 Chongming Island (Tang et al., 2018; Qin et al., 2020; Wang et al., 2020; Wu et al., 2020), which suggests  
365 a heavy GEM pollution on a large regional scale during 2015. The high GEM in January 2015 were most  
366 likely linked to an adverse effect of meteorological conditions due to extreme 2015 – 2016 El Niño event,  
367 which affected the levels of atmospheric pollutants directly via changing precipitation and large-scale air  
368 circulation patterns or indirectly via impacting emissions (e.g. biomass burning) and re-emissions from  
369 land/ocean (Monks et al., 2012; Carbone et al., 2016; Martin et al., 2017; Rowlinson et al., 2019; Yu et  
370 al., 2019; Nguyen et al., 2022).

371 As shown in Fig. 5, the potential source regions of GEM in July were classified to Local, South China  
372 Sea (SCS), Philippines Sea and Taiwan Strait (PhiS+TW), as well as Philippines Sea and East China Sea  
373 (PhiS+ECS). The dominant clean marine air masses helped explain the lower concentration of GEM in  
374 July than in January. The air masses arriving in Xiamen in July were mainly from the SCS and PhiS+TW,  
375 accounting for more than 85% of the total trajectories (except 2015). The weighted average contributions  
376 of GEM from the SCS were 21.4% in July 2015 and 36.1% in July 2017 (Table 2), however, the GEM  
377 concentrations associating with the SCS were approximately 1.29 and 1.13 times higher than the average  
378 GEM in July of 2015 and 2017. Thus, the elevated GEM concentrations of the SCS in July 2015 is due  
379 to that the air masses passed more closely through Southeast Asia where the intense biomass burning  
380 often occurred (Friedli et al., 2009; Sheu et al., 2013; Liu et al., 2016). A previous study on Hainan Island  
381 also pointed to the possibility of long-range transport of GEM from Southeast Asia to South China (Liu  
382 et al., 2016). Very differently, the high GEM of the SCS in July 2017 is likely because the air mass cluster  
383 from the SCS was short which indicates a stagnant air condition, and the air mass cluster was close to  
384 the land of Southeast China where were densely populated and highly industrialized (Yuan et al., 2021).



385 **Table 2. Concentrations (ng m<sup>-3</sup>) and weighted average contributions (%) of GEM associating with**  
 386 **different backward trajectory clusters in January and July over the study years.**

Period	GEM	Source regions				
		Local	EC	NC	SWC	CC
2012.01	3.50±0.62	3.21±0.62 (39.6%)	3.72±0.53 (60.5%)	/	/	/
2013.01	4.01±1.34	4.37±1.33 (30.3%)	4.02±1.34 (63.5%)	2.91±0.69 (6.0%)	/	/
2015.01	4.47±0.78	5.05±0.96 (47.0%)	4.31±0.50 (30.0%)	4.32±0.54 (14.8%)	3.74±0.26 (8.2%)	/
2017.01	4.03±1.00	4.12±1.06 (45.1%)	3.76±1.03 (15.1%)	/	3.93±0.82 (10.0%)	4.12±0.94 (29.9%)
2020.01	3.93±0.88	4.18±1.01 (34.6%)	4.00±0.81 (42.4%)	3.43±0.64 (15.7%)	3.71±0.69 (7.5%)	/
		Local	SCS	PhiS+TW	PhiS+ECS	
2012.07	2.49±0.79	/	2.83±0.85 (57.0%)	2.14±0.63 (30.2%)	2.19±0.41 (12.9%)	
2013.07	2.18±0.65	/	2.11±0.67 (35.4%)	2.23±0.66 (64.4%)	/	
2015.07	2.55±0.86	2.38±0.77 (47.7%)	3.30±0.68 (21.4%)	/	2.18±0.56 (30.8%)	
2017.07	2.65±0.69	/	3.00±0.81 (36.1%)	2.47±0.54 (63.9%)	/	
2020.07	1.56±0.55	/	1.54±0.54 (80.6%)	1.75±0.62 (19.2%)	/	



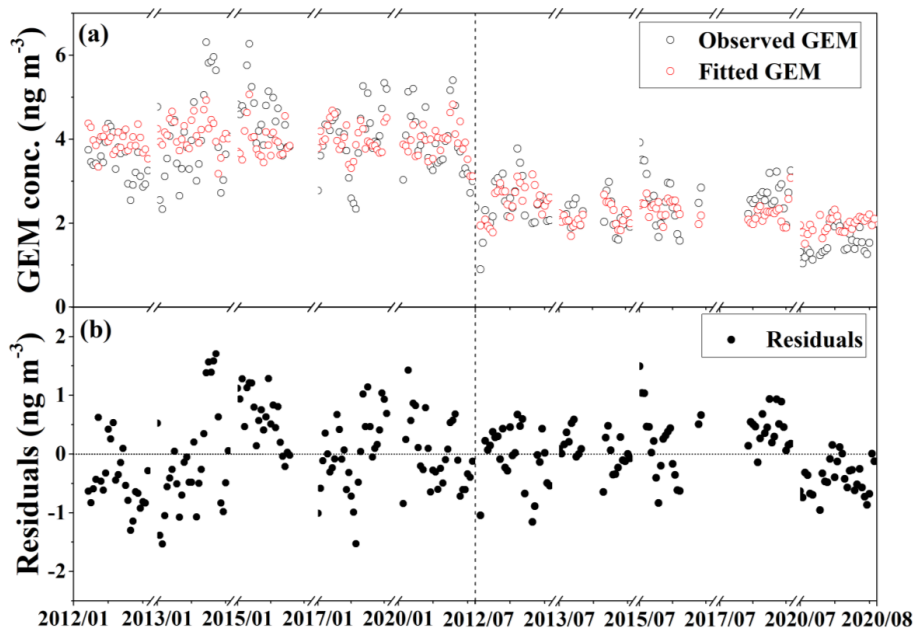
387  
 388 Figure 5. Clusters of 72 h air mass backward trajectories in January (a, c, e, g, i) and July (b, d, f, h, j) during  
 389 the study years. The legend represents the proportion of the trajectory after clustering and the color piece on  
 390 behalf of the source regions.



391 **3.3 Factors affecting GEM concentrations**

392 **3.3.1 Model evaluation**

393 GAMs were applied to investigate the influencing factors on the inter-annual trend of GEM in this  
394 study. The fitted (observed) GEM concentrations derived from the GAMs were approximately  $4.00 \pm$   
395  $0.45 \text{ ng m}^{-3}$  ( $4.00 \pm 0.84 \text{ ng m}^{-3}$ ) in January and  $2.23 \pm 0.33 \text{ ng m}^{-3}$  ( $2.23 \pm 0.61 \text{ ng m}^{-3}$ ) in July, reflecting  
396 that the model approximates the concentration of GEM to the mean. The observed and fitted GEM  
397 concentrations showed a good consistency in time series (Fig. 6a) and the residuals were normally  
398 distributed (Fig. 6b). The  $R^2$  of the observed and fitted GEM concentrations was 0.71 (Fig. S4) and the  
399 variance interpretation rate was 72.3%. In previous studies using GAMs to quantify impact factors on air  
400 pollutants, the  $R^2$  was generally between 0.35 and 0.86 (Gong et al., 2018; Li et al., 2019; Wu et al., 2020;  
401 Wu et al., 2021; Zhang et al., 2021). The fitted result of the GAMs in our study falls in this range.

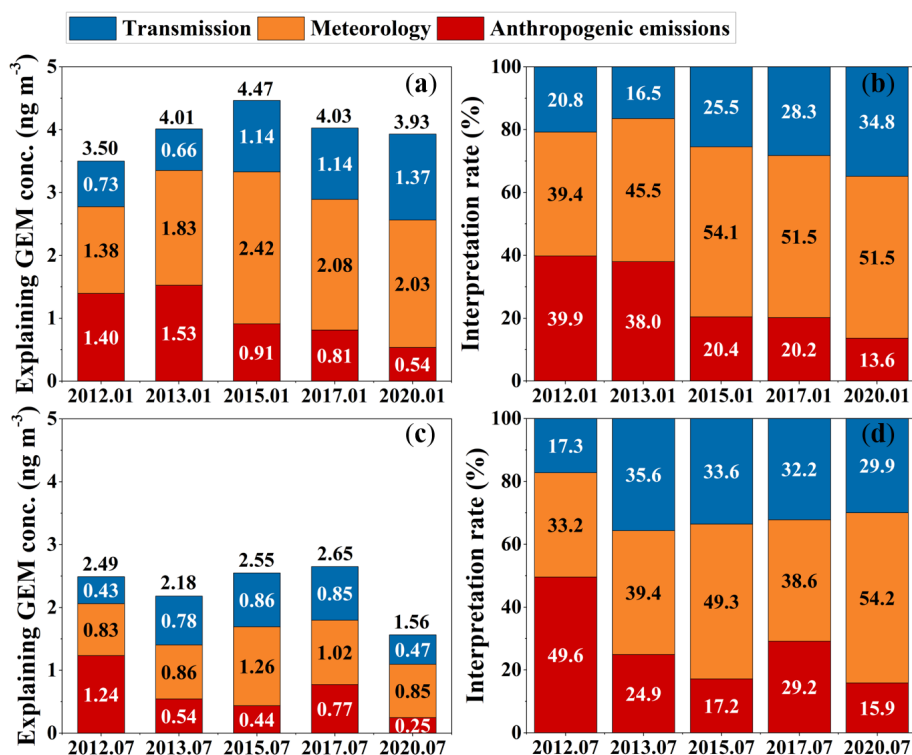


402  
403 **Figure 6.** Time series of (a) observed and fitted GEM concentrations in January and July and (b) residual  
404 distribution during the whole study period.



405 **3.3.2 Inter-annual variations of factor contributions**

406 The GAMs screened out five variables, CO, RH and SP, as well as 24h-Latitude and 24h-Longitude,  
407 which represented three factors of anthropogenic emissions, meteorology and transmission, respectively.  
408 The contributions of the three factors to the variation of GEM concentrations in January and July of the  
409 study years are shown in Fig. 7. The inter-annual interpretation rate of anthropogenic emissions varied  
410 from 13.6% to 39.9% in January and from 15.9% to 49.6% in July, with a mean value of  $26.9 \pm 11.4\%$   
411 during the whole study period. The interpretation rate of the emission factor to the variation of GEM  
412 concentrations was pronouncedly high in 2012 and decreased overall to 2020, which reflects the  
413 effectiveness of emission mitigation measures in reducing GEM concentrations. China has adopted a  
414 series of desulphurization and denitrification measures for air pollution control during the period 2010 –  
415 2015. The capacity of desulphurization and denitrification units in China had reached 99% and 92% of  
416 the total installed capacity of coal power plants, and  $1.6 \times 10^8$  kw had been upgraded to achieve ultra-low  
417 emissions by 2015. In addition, strict restrictions of mercury on the mining, production, use, import and  
418 export were also be imposed in China since 2017 (<http://www.mee.gov.cn>, last access: 17 May 2022).  
419 We observed a positive relationship between GEM and variable CO in most of the CO observed range  
420 (Fig. 8a). That is, GEM concentrations basically decreased with the reduction of CO which stands for  
421 anthropogenic emissions. The most significant reduction in GEM concentrations explained by  
422 anthropogenic emissions was  $0.70 \text{ ng m}^{-3}$  from July 2012 to July 2013 and  $0.62 \text{ ng m}^{-3}$  from January  
423 2013 to January 2015. After that, the effect of anthropogenic emissions on reducing GEM concentrations  
424 gradually diminished. The results indicate that, when the anthropogenic Hg emissions reach a relatively  
425 low level, the influence of emission reduction on GEM concentrations becomes less pronounced, and in  
426 turn, the influence of meteorology and transmission gradually become prominent.



427

428

429

**Figure 7.** The explaining concentration (ng m<sup>-3</sup>) (a, c) and interpretation rate (%) (b, d) of the three factors to the variation of GEM concentrations during the study years.

430

431

432

433

434

435

436

437

438

439

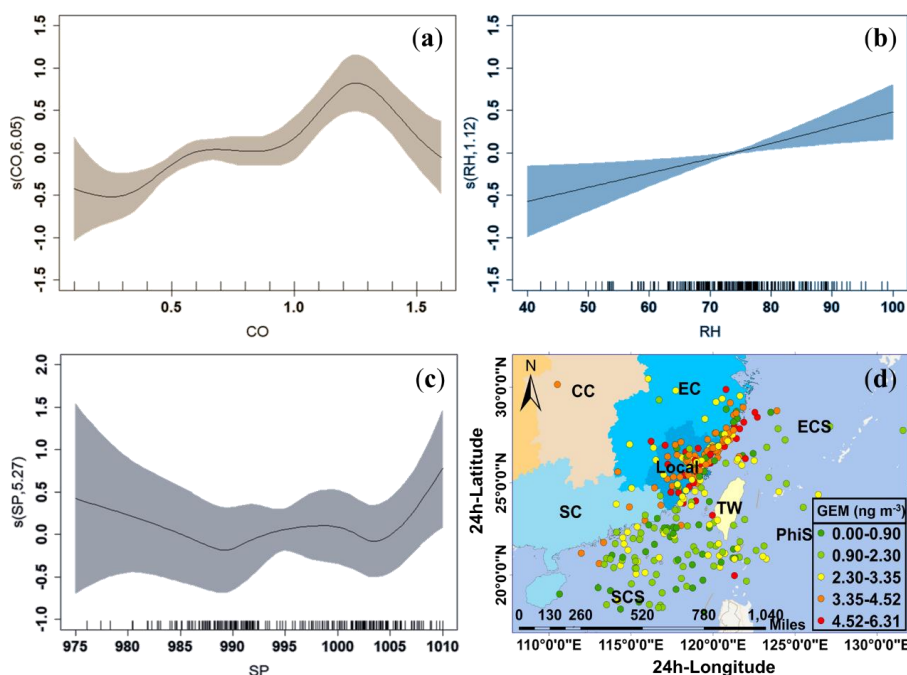
440

441

Meteorology was the most important of the three factors, which contributed, on average,  $45.7 \pm 7.2\%$  to the variation of GEM concentrations during the whole study period. The inter-annual interpretation rate of meteorology largely varied from 39.4% to 54.1% in January and from 33.2% to 54.2% in July. The largest part of GEM concentrations explained by meteorological factor occurred in 2015, which were 2.42 ng m<sup>-3</sup> in January and 1.26 ng m<sup>-3</sup> in July, respectively. According to the importance index F value (Table S2), RH and SP were the two most important parameters for the meteorological factor. As shown in Fig. 8b and 8c, GEM concentrations linearly increased with the increasing RH, while the relationship between GEM and SP was negative when  $SP < 990$  hPa (mostly in July) and positive when  $SP > 1004$  hPa (mostly in January). Thus, in January 2015, the RH and SP both had positive impacts on GEM concentrations, and we suspected that the highest SP (Table S5) could largely explain the high GEM concentrations in this period. The high interpretation rate of meteorological factor in July 2015 was mainly related to the remarkable high RH (82.4%) and low SP compared to the July of other years (Table



442 S5). The quite different meteorological parameters in 2015 from other years were likely driven by the  
443 extreme 2015 – 2016 El Niño event, which led to the elevated GEM concentrations on a regional scale  
444 as mentioned above.



445  
446 **Figure 8. Spline of GEM to the chosen variables, (a) CO (mg m<sup>-3</sup>), (b) RH (%), (c) SP (hPa), and (d) 24h-**  
447 **Longitude, 24h-Latitude. The grey background around the line is 95% confidence bounds for the response.**  
448 **The short lines on x axes show the distribution of data points. The number in the bracket of ordinate title is**  
449 **the estimated degree of freedom. The colored dots in figure (d) represents the interactive influence of 24h**  
450 **backward trajectories latitude and longitude coordinates.**

451 Regional transmission explained a proportion of GEM concentrations comparable to anthropogenic  
452 emissions, which made up  $27.4 \pm 6.8\%$  of total variation during the whole study period. During the period  
453 of 2013 – 2020, the interpretation rate of transmission displayed an increasing trend from 16.5% to 34.8%  
454 in January and a minor variation between 29.9% and 35.6% in July. The interaction of 24 h backward  
455 trajectories location and corresponding GEM concentrations are shown in Fig. 8d. The high GEM  
456 concentrations mostly presented in the areas with 24h-Longitude of 116 – 124°E and 24h-Latitude of 24  
457 – 30°N. This is consistent with the backward trajectory results in section 3.3.2 that the main source  
458 regions of GEM were local area and East China. The interpretation rate of transmission increased



459 significantly in winter among years, indicating the growing importance of transmission from high Hg  
460 emission zone to low emission zone in the background of anthropogenic emissions reduction. This  
461 phenomenon well reflects the characteristics of GEM that undergoes long-range transport.

#### 462 **4 Conclusions**

463 Long-term observation of GEM concentrations along with conventional pollutants and meteorological  
464 parameters were conducted in Xiamen city, Southeast China. GEM concentrations showed no distinct  
465 trends over the period 2012 – 2020. The temporal variation of GEM was characterized by higher values  
466 in winter than in summer and in nighttime than in daytime, which is consistent with those in most urban  
467 cities.

468 Local point sources contributed to the elevated GEM concentrations in individual seasons.  
469 Nevertheless, the inter-annual variation trend of GEM was not consistent with those of local SO<sub>2</sub> and  
470 NO<sub>x</sub> emissions, suggesting that anthropogenic emissions might be not the dominant influencing factor.  
471 The trajectory results showed that the pronounced high GEM concentrations in winter 2015 was a  
472 regional phenomenon, which was likely due to an adverse effect of meteorology due to extreme 2015 –  
473 2016 El Niño event.

474 Three factors, i.e. anthropogenic emissions, meteorological conditions and transmission were  
475 identified by GAMs, which explained  $26.9 \pm 11.4\%$ ,  $45.7 \pm 7.2\%$  and  $27.4 \pm 6.8\%$  to the variation of  
476 GEM concentrations during the whole study period, respectively. Anthropogenic emissions showed a  
477 decreasing interpretation rate since 2012, indicating the effectiveness of emission mitigation measures in  
478 reducing GEM concentrations in the study region. In contrast, the interpretation rate of transmission in  
479 winter displayed an increasing trend. Meteorology explained the largest proportion of GEM  
480 concentrations, which was more likely the dominant factor influencing the inter-annual variation trend  
481 of GEM in the study region.



482 **Data availability.** A dataset for this paper can be accessed at <https://doi.org/10.5281/zenodo.6573605>  
483 (Shi et al., 2022). High-altitude meteorology parameters can be acquired from the European Centre for  
484 Medium-Range Weather Forecasts (ECMWF) reanalysis (<https://www.ecmwf.int>, last access: last access:  
485 23 March 2022), Gridded meteorological data are available from the Global Data Assimilation System  
486 (<https://www.arl.noaa.gov/>, last access:5 May 2022), The details are also available upon request from the  
487 corresponding author.

488

489 **Author contributions.** JS and LX designed this study and analysis the data. YuC, LX, YH, ML, XF,  
490 YaC, CY GC, LT, JX and JC were involved in the scientific discussion and offered valuable suggestions  
491 for modifications. JS and LX wrote the manuscript. YuC and JC helped revise the manuscript. and LY  
492 managed finances. All authors reviewed the paper.

493

494 **Competing interests.** The authors declare that they have no conflict of interest.

495

496 **Disclaimer.** Publisher's note. Copernicus Publications remains neutral with regard to jurisdictional  
497 claims in published maps and institutional affiliations.

498

499 **Acknowledgements.** We would like to thank the Xiamen Atmospheric Environment Observation and  
500 Research Station of Fujian Province for providing data support for this research. We would like to thank  
501 Siqing Zhang, for his help with the daily maintenance of the Tekran system. We also thank the members  
502 of the Atmospheric Environment Research Group of the Urban Environment Institute for their help and  
503 support in data analysis.

504

505 **Financial support.** This research was supported by National Natural Science Foundation of China (grant  
506 no. 21507127; 41575146), the CAS Center for Excellence in Regional Atmospheric Environment (grant  
507 no. E0L1B20201), and Xiamen Atmospheric Environment Observation and Research Station of Fujian  
508 Province.



509 **References**

- 510 Arctic Monitoring and Assessment Programme and United Nations Environment Programme  
511 (AMAP/UNEP): Global mercury assessment 2018 – draft technical background document,  
512 AMAP/UNEP, Geneva, Switzerland, 2018.
- 513 Axelrad, D. A., Bellinger, D. C., Ryan, L. M., and Woodruff, T. J.: Dose-response relationship of prenatal  
514 mercury exposure and IQ: an integrative analysis of epidemiologic data, *Environ Health Perspect*,  
515 115, 609-615, <https://doi.org/10.1289/ehp.9303>, 2007.
- 516 Cai, X. R., Cai, B. F., Zhang, H. R., Chen, L., Zheng, C. Y., Tong, P. F., Lin, H. M., Zhang, Q. R., Liu,  
517 M. D., Tong, Y. D., and Wang, X. J.: Establishment of High-Resolution Atmospheric Mercury  
518 Emission Inventories for Chinese Cement Plants Based on the Mass Balance Method,  
519 *Environmental Science & Technology*, 54, 13399-13408, <https://doi.org/10.1021/acs.est.0c02963>,  
520 2020.
- 521 Carbone, F., Landis, M. S., Gencarelli, C. N., Naccarato, A., Sprovieri, F., De Simone, F., Hedgecock, I.  
522 M., and Pirrone, N.: Sea surface temperature variation linked to elemental mercury concentrations  
523 measured on Mauna Loa, *Geophysical Research Letters*, 43, 7751-7757,  
524 <https://doi.org/10.1002/2016gl069252>, 2016.
- 525 Chen, L., Liu, M., Xu, Z., Fan, R., Tao, J., Chen, D., Zhang, D., Xie, D., and Sun, J.: Variation trends  
526 and influencing factors of total gaseous mercury in the Pearl River Delta—A highly industrialised  
527 region in South China influenced by seasonal monsoons, *Atmospheric Environment*, 77, 757-766,  
528 <https://doi.org/10.1016/j.atmosenv.2013.05.053>, 2013.
- 529 Custodio, D., Ebinghaus, R., Spain, T. G., and Bieser, J.: Source apportionment of atmospheric mercury  
530 in the remote marine atmosphere: Mace Head GAW station, Irish western coast, *Atmospheric*  
531 *Chemistry and Physics*, 20, 7929-7939, <https://doi.org/10.5194/acp-20-7929-2020>, 2020.
- 532 Draxler, R. R.: HYSPLIT4 User's Guide, NOAA Technical Memorandum ERL ARL-230, 1999.
- 533 Duan, L., Wang, X., Wang, D., Duan, Y., Cheng, N., and Xiu, G.: Atmospheric mercury speciation in  
534 Shanghai, China, *Sci Total Environ*, 578, 460-468, <https://doi.org/10.1016/j.scitotenv.2016.10.209>,  
535 2017.
- 536 UN Environment: Financial Rules for the Minamata Convention on Mercury, United Nations  
537 Environment Programme, Geneva, Switzerland,  
538 <https://www.mercuryconvention.org/en/resources/financial-rules-minamata-convention-mercury>,  
539 2017.
- 540 Fang, G. C., Lo, C. T., Cho, M. H., Zhuang, Y. J., Tsai, K. H., Huang, C. Y., and Xiao, Y. F.: Annual  
541 ambient atmospheric mercury speciation measurement from Longjing, a rural site in Taiwan,  
542 *Environ Geochem Health*, 39, 901-911, <https://doi.org/10.1007/s10653-016-9861-x>, 2017.
- 543 Feng, X., Shang, L., Wang, S., Tang, S., and Zheng, W.: Temporal variation of total gaseous mercury in  
544 the air of Guiyang, China, *Journal of Geophysical Research: Atmospheres*, 109, n/a-n/a,  
545 <https://doi.org/10.1029/2003jd004159>, 2004.
- 546 Friedli, H. R., Arellano, A. F., Cinnirella, S., and Pirrone, N.: Initial estimates of mercury emissions to  
547 the atmosphere from global biomass burning, *Environ Sci Technol*, 43, 3507-3513,  
548 <https://doi.org/10.1021/es802703g>, 2009.



- 549 Fu, X., Feng, X., Zhu, W., Wang, S., and Lu, J.: Total gaseous mercury concentrations in ambient air in  
550 the eastern slope of Mt. Gongga, South-Eastern fringe of the Tibetan plateau, China, *Atmospheric*  
551 *Environment*, 42, 970-979, <https://doi.org/10.1016/j.atmosenv.2007.10.018>, 2008.
- 552 Fu, X. W., Zhang, H., Yu, B., Wang, X., Lin, C. J., and Feng, X. B.: Observations of atmospheric mercury  
553 in China: a critical review, *Atmospheric Chemistry and Physics*, 15, 9455-9476,  
554 <https://doi.org/10.5194/acp-15-9455-2015>, 2015.
- 555 Fu, X. W., Feng, X., Liang, P., Deliger, Zhang, H., Ji, J., and Liu, P.: Temporal trend and sources of  
556 speciated atmospheric mercury at Waliguan GAW station, Northwestern China, *Atmospheric*  
557 *Chemistry and Physics*, 12, 1951-1964, <https://doi.org/10.5194/acp-12-1951-2012>, 2012.
- 558 Gong, X., Hong, S., and Jaffe, D. A.: Ozone in China: Spatial Distribution and Leading Meteorological  
559 Factors Controlling O3 in 16 Chinese Cities, *Aerosol and Air Quality Research*, 18, 2287-2300,  
560 <https://doi.org/10.4209/aaqr.2017.10.0368>, 2018.
- 561 Gong, X., Kaulfus, A., Nair, U., and Jaffe, D. A.: Quantifying O3 Impacts in Urban Areas Due to  
562 Wildfires Using a Generalized Additive Model, *Environ Sci Technol*, 51, 13216-13223,  
563 <https://doi.org/10.1021/acs.est.7b03130>, 2017.
- 564 Hong, Q., Xie, Z., Liu, C., Wang, F., Xie, P., Kang, H., Xu, J., Wang, J., Wu, F., He, P., Mou, F., Fan,  
565 S., Dong, Y., Zhan, H., Yu, X., Chi, X., and Liu, J.: Speciated atmospheric mercury on haze and  
566 non-haze days in an inland city in China, *Atmospheric Chemistry and Physics*, 16, 13807-13821,  
567 <https://doi.org/10.5194/acp-16-13807-2016>, 2016a.
- 568 Hong, Y., Chen, J., Deng, J., Tong, L., Xu, L., Niu, Z., Yin, L., Chen, Y., and Hong, Z.: Pattern of  
569 atmospheric mercury speciation during episodes of elevated PM2.5 levels in a coastal city in the  
570 Yangtze River Delta, China, *Environ Pollut*, 218, 259-268,  
571 <https://doi.org/10.1016/j.envpol.2016.06.073>, 2016b.
- 572 Lee, G.-S., Kim, P.-R., Han, Y.-J., Holsen, T. M., Seo, Y.-S., and Yi, S.-M.: Atmospheric speciated  
573 mercury concentrations on an island between China and Korea: sources and transport pathways,  
574 *Atmospheric Chemistry and Physics*, 16, 4119-4133, <https://doi.org/10.5194/acp-16-4119-2016>,  
575 2016.
- 576 Lee, S.-H., Lee, J.-I., Kim, P.-R., Kim, D.-Y., Jeon, J.-W., and Han, Y.-J.: Factors influencing  
577 concentrations of atmospheric speciated mercury measured at the farthest island West of South  
578 Korea, *Atmospheric Environment*, 213, 239-249, <https://doi.org/10.1016/j.atmosenv.2019.05.063>,  
579 2019.
- 580 Li, K., Jacob, D. J., Liao, H., Shen, L., Zhang, Q., and Bates, K. H.: Anthropogenic drivers of 2013-2017  
581 trends in summer surface ozone in China, *Proc Natl Acad Sci U S A*, 116, 422-427,  
582 <https://doi.org/10.1073/pnas.1812168116>, 2019.
- 583 Lindberg, S., Bullock, R., Ebinghaus, R., Engstrom, D., Feng, X. B., Fitzgerald, W., Pirrone, N., Prestbo,  
584 E., and Seigneur, C.: A synthesis of progress and uncertainties in attributing the sources of mercury  
585 in deposition, *Ambio*, 36, 19-32, [https://doi.org/10.1579/0044-7447\(2007\)36\[19:Asopau\]2.0.Co;2](https://doi.org/10.1579/0044-7447(2007)36[19:Asopau]2.0.Co;2),  
586 2007.
- 587 Liu, C., Fu, X., Zhang, H., Ming, L., Xu, H., Zhang, L., and Feng, X.: Sources and outflows of  
588 atmospheric mercury at Mt. Changbai, northeastern China, *Sci Total Environ*, 663, 275-284,  
589 <https://doi.org/10.1016/j.scitotenv.2019.01.332>, 2019a.



- 590 Liu, K., Wang, S., Wu, Q., Wang, L., Ma, Q., Zhang, L., Li, G., Tian, H., Duan, L., and Hao, J.: A Highly  
591 Resolved Mercury Emission Inventory of Chinese Coal-Fired Power Plants, *Environmental Science  
592 & Technology*, 52, 2400-2408, <https://doi.org/10.1021/acs.est.7b06209>, 2018.
- 593 Liu, K., Wu, Q., Wang, L., Wang, S., Liu, T., Ding, D., Tang, Y., Li, G., Tian, H., Duan, L., Wang, X.,  
594 Fu, X., Feng, X., and Hao, J.: Measure-Specific Effectiveness of Air Pollution Control on China's  
595 Atmospheric Mercury Concentration and Deposition during 2013-2017, *Environ Sci Technol*, 53,  
596 8938-8946, <https://doi.org/10.1021/acs.est.9b02428>, 2019b.
- 597 Liu, M., Chen, L., Xie, D., Sun, J., He, Q., Cai, L., Gao, Z., and Zhang, Y.: Monsoon-driven transport of  
598 atmospheric mercury to the South China Sea from the Chinese mainland and Southeast Asia-  
599 Observation of gaseous elemental mercury at a background station in South China, *Environmental  
600 Science and Pollution Research*, 23, 21631-21640, <https://doi.org/10.1007/s11356-016-7432-4>,  
601 2016.
- 602 Martin, L. G., Labuschagne, C., Brunke, E.-G., Weigelt, A., Ebinghaus, R., and Slemr, F.: Trend of  
603 atmospheric mercury concentrations at Cape Point for 1995-2004 and since 2007, *Atmospheric  
604 Chemistry and Physics*, 17, 2393-2399, <https://doi.org/10.5194/acp-17-2393-2017>, 2017.
- 605 Marumoto, K., Hayashi, M., and Takami, A.: Atmospheric mercury concentrations at two sites in the  
606 Kyushu Islands, Japan, and evidence of long-range transport from East Asia, *Atmospheric  
607 Environment*, 117, 147-155, <https://doi.org/10.1016/j.atmosenv.2015.07.019>, 2015.
- 608 Monks, S. A., Arnold, S. R., and Chipperfield, M. P.: Evidence for El Niño-Southern Oscillation (ENSO)  
609 influence on Arctic CO interannual variability through biomass burning emissions, *Geophysical  
610 Research Letters*, 39, n/a-n/a, <https://doi.org/10.1029/2012gl052512>, 2012.
- 611 Nguyen, L. S. P., Nguyen, K. T., Griffith, S. M., Sheu, G. R., Yen, M. C., Chang, S. C., and Lin, N. H.:  
612 Multiscale Temporal Variations of Atmospheric Mercury Distinguished by the Hilbert-Huang  
613 Transform Analysis Reveals Multiple El Niño-Southern Oscillation Links, *Environ Sci Technol*, 56,  
614 1423-1432, <https://doi.org/10.1021/acs.est.1c03819>, 2022.
- 615 Qin, X., Wang, X., Shi, Y., Yu, G., Zhao, N., Lin, Y., Fu, Q., Wang, D., Xie, Z., Deng, C., and Huang,  
616 K.: Characteristics of atmospheric mercury in a suburban area of east China: sources, formation  
617 mechanisms, and regional transport, *Atmospheric Chemistry and Physics*, 19, 5923-5940,  
618 <https://doi.org/10.5194/acp-19-5923-2019>, 2019.
- 619 Qin, X., Zhang, L., Wang, G., Wang, X., Fu, Q., Xu, J., Li, H., Chen, J., Zhao, Q., Lin, Y., Huo, J., Wang,  
620 F., Huang, K., and Deng, C.: Assessing contributions of natural surface and anthropogenic  
621 emissions to atmospheric mercury in a fast-developing region of eastern China from 2015 to 2018,  
622 *Atmospheric Chemistry and Physics*, 20, 10985-10996, <https://doi.org/10.5194/acp-20-10985-2020>,  
623 2020.
- 624 Qiu, Y., Gai, P., Yue, F., Zhang, Y., He, P., Kang, H., Yu, X., Lam, P. K. S., Chen, J., and Xie, Z.: Stable  
625 Mercury Isotopes Revealing Photochemical Processes in the Marine Boundary Layer, *Journal of  
626 Geophysical Research: Atmospheres*, 126, <https://doi.org/10.1029/2021jd034630>, 2021.
- 627 Rallo, M., Lopez-Anton, M. A., Contreras, M. L., and Maroto-Valer, M. M.: Mercury policy and  
628 regulations for coal-fired power plants, *Environ Sci Pollut Res Int*, 19, 1084-1096,  
629 <https://doi.org/10.1007/s11356-011-0658-2>, 2012.
- 630 Roman, H. A., Walsh, T. L., Coull, B. A., Dewailly, E., Guallar, E., Hattis, D., Marien, K., Schwartz, J.,  
631 Stern, A. H., Virtanen, J. K., and Rice, G.: Evaluation of the cardiovascular effects of



- 632 methylmercury exposures: current evidence supports development of a dose-response function for  
633 regulatory benefits analysis, *Environ Health Perspect*, 119, 607-614,  
634 <https://doi.org/10.1289/ehp.1003012>, 2011.
- 635 Rowlinson, M. J., Rap, A., Arnold, S. R., Pope, R. J., Chipperfield, M. P., McNorton, J., Forster, P.,  
636 Gordon, H., Pringle, K. J., Feng, W., Kerridge, B. J., Latter, B. L., and Siddans, R.: Impact of El  
637 Niño–Southern Oscillation on the interannual variability of methane and tropospheric ozone,  
638 *Atmospheric Chemistry and Physics*, 19, 8669-8686, <https://doi.org/10.5194/acp-19-8669-2019>,  
639 2019.
- 640 Schroeder, W. H. and Munthe, J.: Atmospheric mercury—An overview, *Atmospheric Environment*, 32,  
641 809-822, [https://doi.org/10.1016/s1352-2310\(97\)00293-8](https://doi.org/10.1016/s1352-2310(97)00293-8), 1998.
- 642 Sheu, G.-R., Phu Nguyen, L. S., Truong, M. T., and Lin, D.-W.: Characteristics of atmospheric mercury  
643 at a suburban site in northern Taiwan and influence of trans-boundary haze events, *Atmospheric*  
644 *Environment*, 214, <https://doi.org/10.1016/j.atmosenv.2019.116827>, 2019.
- 645 Sheu, G.-R., Lin, N.-H., Lee, C.-T., Wang, J.-L., Chuang, M.-T., Wang, S.-H., Chi, K. H., and Ou-Yang,  
646 C.-F.: Distribution of atmospheric mercury in northern Southeast Asia and South China Sea during  
647 Dongsha Experiment, *Atmospheric Environment*, 78, 174-183,  
648 <https://doi.org/10.1016/j.atmosenv.2012.07.002>, 2013.
- 649 Shi, J., Chen, Y., Xu, L., Hong, Y., Li, M., Fan, X., Yin, L., Chen, Y., Yang, C., Chen, G., Liu, T., Ji, X.,  
650 and Chen, J.: Measurement report: Atmospheric mercury in a coastal city of Southeast China: inter-  
651 annual variations and influencing factors, Zenodo [data set],  
652 <https://doi.org/10.5281/zenodo.6573605>, 2022.
- 653 Slemr, F., Martin, L., Labuschagne, C., Mkololo, T., Angot, H., Magand, O., Dommergue, A., Garat, P.,  
654 Ramonet, M., and Bieser, J.: Atmospheric mercury in the Southern Hemisphere – Part I: Trend and  
655 inter-annual variations in atmospheric mercury at Cape Point, South Africa, in 2007–2017, and on  
656 Amsterdam Island in 2012–2017, *Atmospheric Chemistry and Physics*, 20, 7683-7692,  
657 <https://doi.org/10.5194/acp-20-7683-2020>, 2020.
- 658 Sprovieri, F., Pirrone, N., Ebinghaus, R., Kock, H., and Dommergue, A.: A review of worldwide  
659 atmospheric mercury measurements, *Atmospheric Chemistry and Physics*, 10, 8245-8265,  
660 <https://doi.org/10.5194/acp-10-8245-2010>, 2010.
- 661 Tang, Y., Wang, S., Wu, Q., Liu, K., Wang, L., Li, S., Gao, W., Zhang, L., Zheng, H., Li, Z., and Hao,  
662 J.: Recent decrease trend of atmospheric mercury concentrations in East China: the influence of  
663 anthropogenic emissions, *Atmospheric Chemistry and Physics*, 18, 8279-8291,  
664 <https://doi.org/10.5194/acp-18-8279-2018>, 2018.
- 665 Tekran: Tekran Model 1130 Mercury Speciation Unit and Model 1135-P Particulate Mercury Unit User  
666 Manual, Toronto, Canada, 2001.
- 667 Wang, C., Wang, Z., and Zhang, X.: Two years measurement of speciated atmospheric mercury in a  
668 typical area of the north coast of China: Sources, temporal variations, and influence of regional and  
669 long-range transport, *Atmospheric Environment*, 228,  
670 <https://doi.org/10.1016/j.atmosenv.2019.117235>, 2020.
- 671 Wang, C., Wang, Z., and Zhang, X.: Speciated atmospheric mercury during haze and non-haze periods  
672 in winter at an urban site in Beijing, China: Pollution characteristics, sources, and causes analyses,  
673 *Atmospheric Research*, 247, <https://doi.org/10.1016/j.atmosres.2020.105209>, 2021.



- 674 Wood, S. N. and Augustin, N. H.: GAMs with integrated model selection using penalized regression  
675 splines and applications to environmental modelling, *Ecol Model*, 157, 157-177,  
676 [https://doi.org/10.1016/S0304-3800\(02\)00193-X](https://doi.org/10.1016/S0304-3800(02)00193-X), 2002.
- 677 Wu, Q., Tang, Y., Wang, S., Li, L., Deng, K., Tang, G., Liu, K., Ding, D., and Zhang, H.: Developing a  
678 statistical model to explain the observed decline of atmospheric mercury, *Atmospheric Environment*,  
679 243, <https://doi.org/10.1016/j.atmosenv.2020.117868>, 2020.
- 680 Wu, Q. R., Wang, S. X., Li, G. L., Liang, S., Lin, C. J., Wang, Y. F., Cai, S. Y., Liu, K. Y., and Hao, J.  
681 M.: Temporal Trend and Spatial Distribution of Speciated Atmospheric Mercury Emissions in  
682 China During 1978-2014, *Environmental Science & Technology*, 50, 13428-13435,  
683 <https://doi.org/10.1021/acs.est.6b04308>, 2016.
- 684 Wu, Q. R., Tang, Y., Wang, L., Wang, S. X., Han, D. M., Ouyang, D. W., Jiang, Y. Q., Xu, P., Xue, Z.  
685 G., and Hu, J. N.: Impact of emission reductions and meteorology changes on atmospheric mercury  
686 concentrations during the COVID-19 lockdown, *Science of the Total Environment*, 750, 7,  
687 <https://doi.org/10.1016/j.scitotenv.2020.142323>, 2021.
- 688 Wu, Y., Wang, S., Streets, D. G., Hao, J., Chan, M., and Jiang, J.: Trends in anthropogenic mercury  
689 emissions in China from 1995 to 2003, *Environ Sci Technol*, 40, 5312-5318,  
690 <https://doi.org/10.1021/es060406x>, 2006.
- 691 Xu, L., Chen, J., Yang, L., Niu, Z., Tong, L., Yin, L., and Chen, Y.: Characteristics and sources of  
692 atmospheric mercury speciation in a coastal city, Xiamen, China, *Chemosphere*, 119, 530-539,  
693 <https://doi.org/10.1016/j.chemosphere.2014.07.024>, 2015.
- 694 Xu, L., Zhang, Y., Tong, L., Chen, Y., Zhao, G., Hong, Y., Xiao, H., and Chen, J.: Gas-particle  
695 partitioning of atmospheric reactive mercury and its contribution to particle bound mercury in a  
696 coastal city of the Yangtze River Delta, China, *Atmospheric Environment*, 239,  
697 <https://doi.org/10.1016/j.atmosenv.2020.117744>, 2020.
- 698 Yi, H., Tong, L., Lin, J.-m., Cai, Q.-l., Wang, K.-q., Dai, X.-r., Li, J.-r., Chen, J.-s., and Xiao, H.:  
699 Temporal variation and long-range transport of gaseous elemental mercury (GEM) over a coastal  
700 site of East China, *Atmospheric Research*, 233, <https://doi.org/10.1016/j.atmosres.2019.104699>,  
701 2020.
- 702 Yin, X., Kang, S., de Foy, B., Ma, Y., Tong, Y., Zhang, W., Wang, X., Zhang, G., and Zhang, Q.: Multi-  
703 year monitoring of atmospheric total gaseous mercury at a remote high-altitude site (Nam Co,  
704 4730 m a.s.l.) in the inland Tibetan Plateau region, *Atmospheric Chemistry and Physics*, 18, 10557-  
705 10574, <https://doi.org/10.5194/acp-18-10557-2018>, 2018.
- 706 Yin, X., Zhou, W., Kang, S., de Foy, B., Yu, Y., Xie, J., Sun, S., Wu, K., and Zhang, Q.: Latest  
707 observations of total gaseous mercury in a megacity (Lanzhou) in northwest China, *Sci Total*  
708 *Environ*, 720, 137494, <https://doi.org/10.1016/j.scitotenv.2020.137494>, 2020.
- 709 Yu, B., Wang, X., Lin, C. J., Fu, X., Zhang, H., Shang, L., and Feng, X.: Characteristics and potential  
710 sources of atmospheric mercury at a subtropical near-coastal site in East China, *Journal of*  
711 *Geophysical Research: Atmospheres*, 120, 8563-8574, <https://doi.org/10.1002/2015jd023425>, 2015.
- 712 Yu, X., Wang, Z., Zhang, H., and Zhao, S.: Impacts of different types and intensities of El Nino events  
713 on winter aerosols over China, *Sci Total Environ*, 655, 766-780,  
714 <https://doi.org/10.1016/j.scitotenv.2018.11.090>, 2019.



- 715 Yuan, C. S., Jhang, Y. M., Ie, I. R., Lee, C. E., Fang, G. C., and Luo, J. J.: Exploratory investigation on  
716 spatiotemporal variation and source identification of atmospheric speciated mercury surrounding  
717 the Taiwan Strait, *Atmospheric Pollution Research*, 12, 54-64,  
718 <https://doi.org/10.1016/j.apr.2021.01.015>, 2021.
- 719 Zhang, H., Fu, X., Lin, C.-J., Shang, L., Zhang, Y., Feng, X., and Lin, C.: Monsoon-facilitated  
720 characteristics and transport of atmospheric mercury at a high-altitude background site in  
721 southwestern China, *Atmospheric Chemistry and Physics*, 16, 13131-13148,  
722 <https://doi.org/10.5194/acp-16-13131-2016>, 2016a.
- 723 Zhang, L., Wang, S. X., Wang, L., and Hao, J. M.: Atmospheric mercury concentration and chemical  
724 speciation at a rural site in Beijing, China: implications of mercury emission sources, *Atmospheric  
725 Chemistry and Physics*, 13, 10505-10516, <https://doi.org/10.5194/acp-13-10505-2013>, 2013.
- 726 Zhang, L., Zhou, P., Zhong, H., Zhao, Y., Dai, L., Wang, Q. g., Xi, M., Lu, Y., and Wang, Y.: Quantifying  
727 the impacts of anthropogenic and natural perturbations on gaseous elemental mercury (GEM) at a  
728 suburban site in eastern China using generalized additive models, *Atmospheric Environment*, 247,  
729 <https://doi.org/10.1016/j.atmosenv.2020.118181>, 2021.
- 730 Zhang, L., Wang, S., Wang, L., Wu, Y., Duan, L., Wu, Q., Wang, F., Yang, M., Yang, H., Hao, J., and  
731 Liu, X.: Updated Emission Inventories for Speciated Atmospheric Mercury from Anthropogenic  
732 Sources in China, *Environmental Science & Technology*, 49, 3185-3194,  
733 <https://doi.org/10.1021/es504840m>, 2015.
- 734 Zhang, Y., Jacob, D. J., Horowitz, H. M., Chen, L., Amos, H. M., Krabbenhoft, D. P., Slemr, F., St Louis,  
735 V. L., and Sunderland, E. M.: Observed decrease in atmospheric mercury explained by global  
736 decline in anthropogenic emissions, *Proc Natl Acad Sci U S A*, 113, 526-531,  
737 <https://doi.org/10.1073/pnas.1516312113>, 2016b.
- 738 Zhu, J., Wang, T., Talbot, R., Mao, H., Hall, C. B., Yang, X., Fu, C., Zhuang, B., Li, S., Han, Y., and  
739 Huang, X.: Characteristics of atmospheric Total Gaseous Mercury (TGM) observed in urban  
740 Nanjing, China, *Atmospheric Chemistry and Physics*, 12, 12103-12118,  
741 <https://doi.org/10.5194/acp-12-12103-2012>, 2012.
- 742
- 743